

Flow Separation Control in Rocket Nozzle

Sarath Pillai¹, Nandu S Kumar², V H Akshay³, Sibin Joju K⁴, C. Pedda Peeraiah⁵

^{1,2,3,4}Final Year B. Tech Students, Dept. of Aeronautical Engineering, ILM College of Engineering & Technology, Ernakulam, Kerala, India

⁵Scientist, Vikram Sarabhai Space Centre (VSSC), Thiruvananthapuram, Kerala, India

Abstract – Modern Rockets generally employ De – Laval nozzle also known as Bell nozzle for producing thrust by expanding the rocket's exhaust gases. Bell nozzles are superior in performance and reliability in terms of length, weight and thrust produced than their counterpart – Conical Nozzles. The bell nozzle has an inherited problem; they are designed to perform at its optimum efficiency at a particular altitude. The bell nozzle generally faces performance issues as they work at off-designed conditions most of the time. The main problem they face is the flow separation phenomenon, which in turn leads to increased side loads, increased vibrations and reduced thrust. There are many methods to address the flow separation issue in the rocket nozzle, among which using secondary flow injection at the lip of nozzle exhaust is one of the methods. This paper researches about changes in flow separation point in a bell nozzle with and without secondary flow injection at the lip of the nozzle's exhaust with the help of ANSYS simulation software. Certain pressure inlet values for the main nozzle are considered and for the secondary nozzle, the pressure inlet values are taken the half of the respective main nozzle pressure inlet values.

Key Words: De – Laval nozzle, off – designed conditions, flow separation, side loads, secondary flow injection.

1. INTRODUCTION

Rocket nozzle produce thrust by expanding the exhaust gases on the virtue of their potential energy. Nozzles are generally categorized into three types – Convergent nozzle, Divergent Nozzle and Convergent – Divergent Nozzle. The rocket uses the Convergent – Divergent nozzle configuration for their ability to produce supersonic exhaust with subsonic flow provided as inlet. The Convergent – Divergent nozzle is again segregated into two types – Conical nozzle and Bell (De – Laval) nozzle. The bell nozzle configuration is more preferred for their performance and reliability. However, the bell nozzles are designed to perform with optimum efficiency at a particular altitude which implies that the nozzles are performing at lower efficiency most of the time owing to functioning at off-design conditions. The off – designing functioning of the nozzle leads to flow separation, which further leads to increases side loads, increased nozzle wall temperature, increased vibrations and reduced thrust.

There are many methods available to control the flow separation phenomenon. This journal researches about the change in flow separation point by providing a secondary

flow injection through a secondary nozzle located near to the main nozzle's exhaust lip.

During the flow separation, the ambient air is sucked inside the nozzle which tends to recharge the re-circulation flow downstream the flow separation. The idea is to prevent the suction of ambient air by providing a secondary flow through the secondary nozzle at the main nozzle lips. The secondary flow will act as a barrier which will block the entry of ambient air, hence reducing the strength of the recirculation zone and reattaching the separated flow back to the nozzle wall.

1.1 Flow separation in rocket nozzle

To understand the flow separation in a rocket nozzle, many numerous experimental and computational tests were conducted. Flow separation generally happens at a certain ratio of chamber pressure to the ambient pressure, which then results in shock formation finally resulting into a complex interaction of shock wave with the boundary layer inside the nozzle.

To understand the flow separation many extensive researches were conducted at the JPL laboratory during 1950's. The authors found that the flow separation in a rocket nozzle will happen if the exhaust pressure is 0.4 times the ambient pressure. This relation is known as "Summerfield criteria".

Generally, there are two types of flow separations, they are as follows:

- I. Free shock separation (FSS) – In this type of flow separation, the flow that detaches from the nozzle wall due to the adverse pressure gradient will never reattach with the nozzle wall. This phenomenon results in increased side loads, increased nozzle wall temperature, increased vibrations and reduced thrust.
- II. Restricted shock separation (RSS) – In this type of flow separation, the flow that detaches from the nozzle wall gets reattached to the nozzle wall downstream the separation point. The reason for the flow reattachment is the diminishing of recirculation flow strength.

2. LITERATURE SURVEY

Beena D. Baloni, Sonu P. Kumar and S.A. Channiwala found various shock wave locations in the diverging section of a designed nozzle for both hot and cold working fluids provided at various NPR [110-9]. Contours of Mach number at pressure inlet 5 bar [110-7].

Luca Boccaletto and Francois Cahuzac designed and analyzed the rocket nozzle having a secondary flow injection at the main nozzle exhaust lip. They simulated and analyzed the flow separation point for a main nozzle having NPR (Nozzle pressure ratio) – 37 bar and providing the secondary nozzle pressure inlet of 6 bar. They compared the location of flow separation point with and without the secondary injection. They were able to achieve full flow condition when using secondary injection [8] - [9]. The figure used in our simulation was referred from [3].

Rokas Simions and Dr. Bidur Khanal conducted simulations of rocket nozzle exhaust plumes at various operating main nozzle pressure inlet conditions. Mainly the nozzle was provided pressure inlet of 8 bar, 20 bar and 31 bar respectively.

3. NOZZLE DESIGN AND GEOMETRY

CATIA, a multiplatform software developed by Dassault Systems is mainly used for computer aided drawing, manufacturing and engineering. It has its own 3D experience platform including surfacing and shape designing, electrical, fluid, mechanical engineering, system engineering and electronic system design.

The conceptual design of main nozzle having secondary nozzle (Aerospike model) designed in CATIA software is given below.

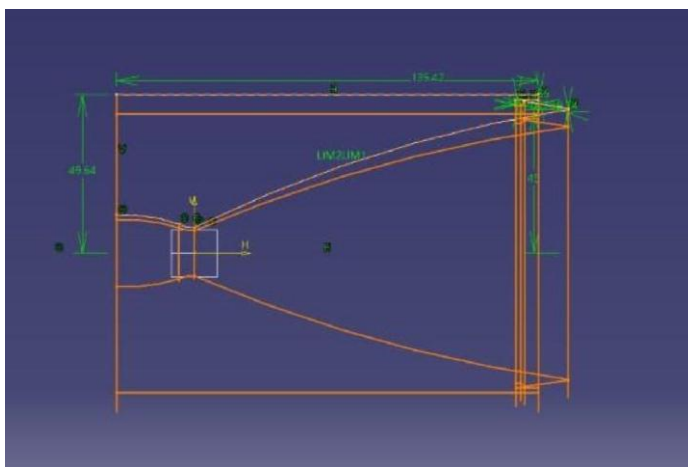


Fig -1: CATIA Sketch

The rough conceptual design sketched in CATIA software is made to produce a three dimensional sketch as shown below.

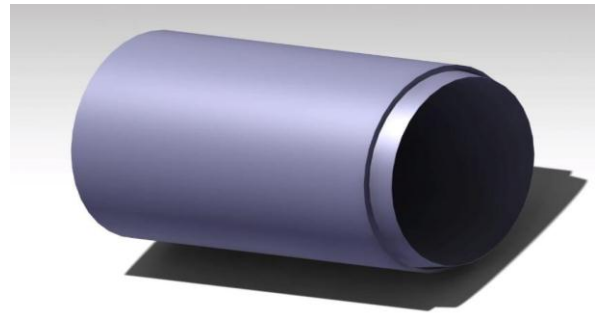


Fig -2: CATIA 3D model

4. ANSYS SIMULATION

ANSYS develop and market engineering simulation software which can be used across the product of life cycle. The computer models of structures, electronics or machine components is done by ANSYS mechanical finite element analysis software. It analyses strength, toughness, elasticity, temperature distribution, electromagnetism, fluid flow and other attributes. ANSYS workbench system is one of the company's main products which performs most ANSYS simulations. Large structures are typically broken down into small components by the ANSYS users that are each modelled and tested individually. The dimensions of an object is defined first by the users, then weight, pressure, temperature and other physical properties are added. In the final stage movement, fatigue, fractures, fluid flow, temperature distribution, electromagnetic efficiency and others effects over time are simulated and analyzed by ANSYS.

4.1 GEOMETRY

The complex geometries are divided into simple elements through meshing which is an integral part of the engineering simulation process. It can be used as discrete local approximations of the larger domain. The accuracy, convergence and the speed of the simulation is influenced by the mesh.

Using the fluid flow (fluent) as the ANSYS workbench tool, the basic analysis of the system is carried out. The geometry is prepared in the Designer Modeler. The surface is sketched by taking the XY Plane as the reference axis, a geometry of the nozzle with 12, 8.07 and 60 being the inlet throat and outlet values which are in millimeters, the inlet and the outlets are 20 and 120 millimeters away from throat.

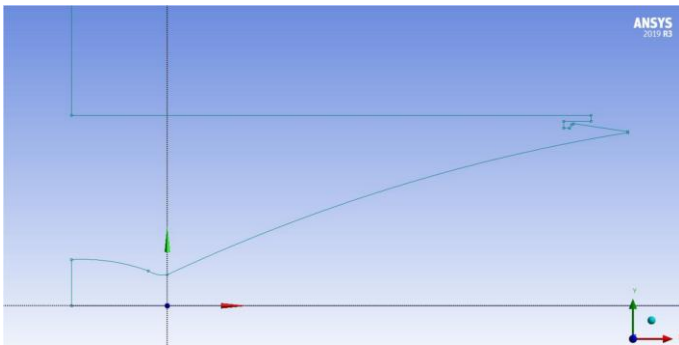


Fig -3: Sketch of CD nozzle with Aerospike

The reduction in flow separation at the exhaust which will be shown at the exhaust plume when the flow takes place is analyzed by the geometry with an inserted aerospike inlet is designed. A secondary Aerospike with (1.79mm) aerospike inlet is designed for the purpose. It supply's the pressure required to reduce the flow separation from the main nozzle. The atmosphere is analyzed by the outer domain which is created by extending 3 times of nozzle size, 600mm width and 3000mm length. To convert the geometry into a developed surface, 'Surface from Sketch' is done which is previewed from the 'concept' bar icon. This surface generation fills the geometry into a complete surface as shown in the below figure.

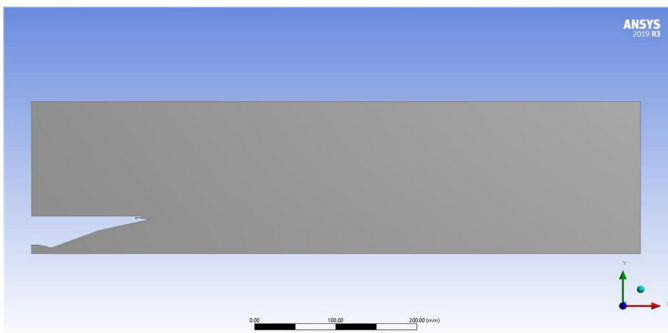


Fig-4: Surface Generated CD Nozzle with Boundary Domain

Face split option is used to face split the generated geometry into different faces. Lines are drawn vertically and horizontally on the generated surface of the geometry for face splitting- then the target face of the geometry is selected by clicking on face split in 'Tools'. The tools geometry is defined as required.

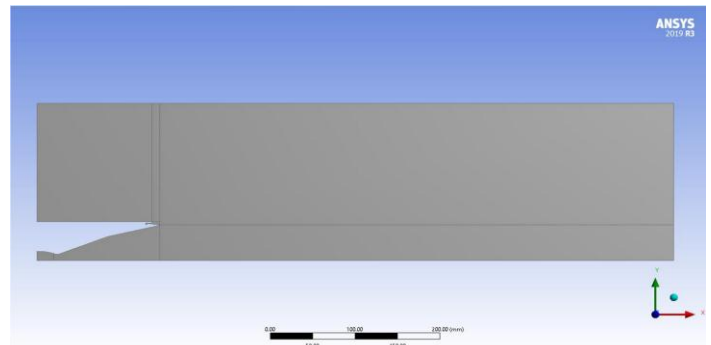


Fig -5: Face split Geometry

4.2 MESHING

Meshing is an integral part of the engineering simulation process where complex geometries are divided into simple elements that can be used as discrete local approximations of the larger domain. The mesh influences the accuracy, convergence and speed of the simulation. Creating the most appropriate mesh is the foundation of engineering simulations.

The display style can be set using geometry setting. The physics preference is CFD and the solver preference is FLUENT. It has a linear element order with element size 0.15297m. The export format is standard with no export preview surface mesh.

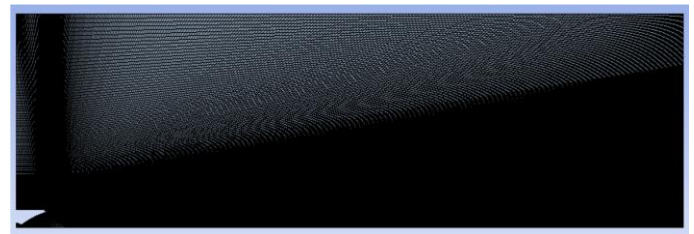


Fig-6: Meshed Geometry

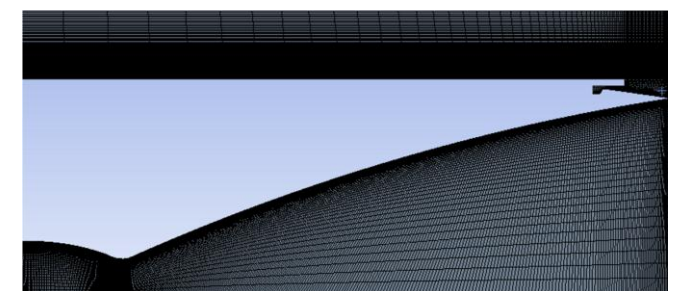


Fig -7: Meshed Nozzle section

The generated mesh has 1.02e-06 wall spacing towards the wall edges for the flow to develop properly, the spacing. This is the inlet of the geometry and using the edge sizing the inlet is well meshed and also the bias factor is applied for the concentration of mesh where detailed analysis is required. Here we are using 40 as the number of division and 30 as the bias factor, also wall is edge sized and the number of division

is 80. In the throat section the edge sizing is 40 and bias factor is 30, the wall is also edge sized to 30. The exit section of the throat wall is edge sized to 250 and the outlet is edge sized to 80 and the bias factor is 60. Using the face meshing option the faces of the geometry is uniform. For the sizing, the element size used for the entire model. We are using advanced size function on Proximity and curvature. The defined relevance center is fine and the smoothing is high. The growth rate is 1.2, because the growth rate has a big impact on the cell count and define the ratio between sizes of adjacent cells. For a growth rate of 1.2, it consists 587026 cells. So we are keeping the growth rate to 1.2. The mesh de-feature is 7.6485e-004m. The capture minimum size is 1.5297e-003m and the curvature normal angle is 18 degrees. There is no capture proximity and the bounding box diagonal is 3.0594m, the average surface area is 0.25668 meter square and the minimum edge length is 2.4711e-004m. The generated mesh has some errors and the target skewness is 0.900000. It has medium smoothing without mesh metric. The inflation is used to generate thin cells adjacent to boundaries or the option to control growth. The inflation option is smooth transition. By using smooth transition, it maintains smooth volumetric growth between each adjacent layer. Total thickness depends on the variation of base surface mesh size. The transition ratio is 0.272, maximum layers is 2 and the growth rate discussed above. The de-featuring removes small geometry meeting the tolerances using pinch in order to improve the mesh quality. The pinch tolerance is 1.3767e-003m. The statistics of the generated mesh follows;

Nodes: 109584

Elements: 108580

Bias option and bias type is the feature that is useful for any engineering problem where nodes need to be clustered on an edge, or if there is a need to bias the mapped mesh of a face towards a specific direction with respect to the edges of the face. The bias type is used to adjust the spacing ratio of nodes on an edge. The three types of bias factor used in the geometry that is no biased condition, right concentrated condition and left concentrated condition in the edge sizing option, we use this type of bias factor for the selected areas for detailed analysis. It helps to analyze the wall of the geometry, aero spike, throat section etc.

4.3 SIMULATION SETTING

For developing flow simulation using ANSYS, different flow properties for each flow forming parameters have to be considered individually. These parameters vary from setting General flow input values to the boundary flow conditioning values.

4.3.1 General Flow Parameters & simulation setup

The nature of the flow used for the simulation of flow separation control in rocket nozzle is assumed to be in a

steady state. Density based solver type, compressible flow as this validates the governing laws of physics and can be used accurately for real time error corrections during iteration run process. The main parameters that are varied to accurately define the flow properties include:

The Energy Equation in the solver is activated. On activating the Energy Equation, the system monitors the level of heat and the impact of heat causing property variations on the fluid molecule (in this case the fluid is air).

The flow direction is specified by naming the zone inlet under the compute from domain. The inlet for flow simulation iterations for the flow analysis is done with values that are manually entered, thus flow fluctuations can be made possible by selecting Standard Initialization setup option from the workbench taskbar.

Viscous characteristics of the flow domain are chosen depending on the velocity of the fluid and area of the contour at that particular point. The viscosity varies from laminar to turbulence or at times can become in-viscid, this can be interpreted by using the Spalart-Allmaras model, Spalart-Allmaras is an equation that is used to solve a modelled transport equation for kinematic eddy or turbulent viscosity basically for low Reynolds number which are suitable for solving flow with varying local shear layer thickness and layers subjected to adverse pressure gradients. The Sutherland's viscosity formula which is based on the relation between temperature and dynamic viscosity helps to sort out higher order flow dimensions involving multiple coefficients thus the Sutherland's viscosity solver is used to solve the contour flow in the project.

For improving the rate of convergence and increasing the stability of the iterative process, Under Relaxation parameter is used. For getting smooth convergence the under relaxation factor must be kept low which aids for the momentum stability thus increases the rate of convergence as shown in figure below.

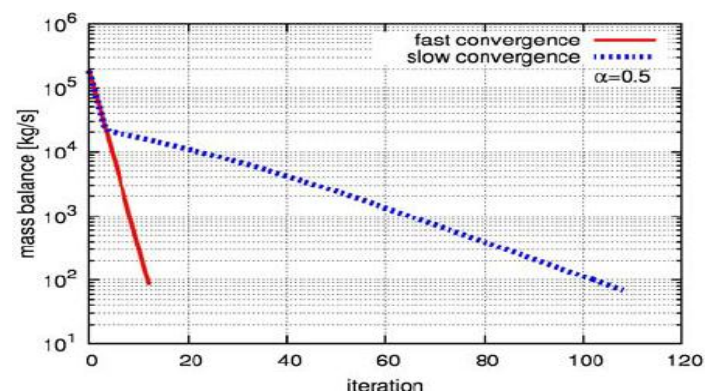


Fig-8: Relaxation cure

4.3.2 Geometric Sectioning

In order to define the fluid flow performance over the surface and to accurately evaluate the flow characteristics throughout the domain, the entire geometry is separated and classified as: The Interior Surface Body which is the working body, the Secondary Injection part which is the prime concern and the boundary surface known also as Pressure Far Field.

Since the project deals with a combination of bell shaped and secondary aero-spike modules of convergent-divergent section. They are meshed differently by sectioning and naming them as; Inlet, Interior Surface Body, Nozzle Wall, Pressure Far Field, Secondary Inlet, Secondary Wall, Surface Body.

4.3.3 Flow Parameters after Geometric Sectioning

The geometric integration of a primary and secondary aero-spike nozzle which is positioned around the main nozzle lip to prevent the penetration of ambient air (even for a pressure difference of 1bar). The entire geometry is thus sectioned accordingly to analyze and understand the flow patterns in each point of the mesh.

The first order upwind type flow is used as the problem is under density based solver type, which are subjected to adverse pressure gradients that depends on the geometry of the sections. To reduce the effect of turbulence Turbulent Viscosity is used as this relates the average shear stress and rate of velocity gradient in turbulent flow to make the flow possibly steady and linear. But due to the geometry it evokes turbulence which increases the boundary growth stiffness and thus requires a large sub surface to understand the impact of boundary layer growth on the system with respect to the atmospheric conditions which is thus named as Pressure Far Field. The values of pressure at the pressure far field is kept constant at 1 atm assuming a standard atmospheric condition.

To get more accurate results the meshed terms are categorized into Spatial Discretization Gradients during the Solution Method preference setup. Spatial Discretization carries out the discretization of convective terms in the solution equation which is based on the Green Gauss Cell, along with the Spatial Discretization a First Order Upwind flow condition gives more stable discretizing scheme. Presence of residuals will however increase the convergence time.

Depending on the severity of the start-up conditions always the value of Courant Number (functions only with a density based solver) should be set to a lower value. The range of Courant Number values will make a given numerical scheme stable; the value is obtained by computing the time stepping scheme. For large time steps the quicker will be the convergence rate.

By noting the flow stimulation, the flow starting from the inlet of the geometry will have more residuals and thus the value of Courant Number is given low, as this lower value enhances the rate of convergence and thereafter the regions computed with lower residuals are given with a higher order Courant Number. This helps to achieve a faster convergence since we are using a multistage scheme with implicit formation this will be stable for courant number up to 2.5 and it is lowered to a value as low as 0.1 to 0.5 and once the start-up transients are reduced the number can be raised again this supports us for the Implicit type formation.

It begins to initialize the computation by activating the 'Run Calculation' command key.

Flow simulation is based on different Initial Input Values of Gauge Pressure and for the evaluation based on input Gauge Pressure Values of 5, 10, 15, 20 and 25 (values in atm) for flow simulation without any secondary injection. The pressure input values for nozzle having secondary injection, the value of main nozzle pressure inlet value is assumed to be 5, 10, 15, 20, 25 (values in atm) and the secondary nozzle pressure inlet is assumed to be half of the pressure inlet taken for main nozzle pressure inlet. Supersonic/Initial pressure gauge can be determined from following relation:

$$\frac{P_0}{P_2} = \left(1 + \frac{(\gamma - 1)}{2} M^2 \right)^{\frac{\gamma}{\gamma - 1}}$$

$$P_2 = \frac{P_0}{factor}$$

Where, P_0 = Total pressure, P_2 = Initial gauge pressure, M = Mach number and γ = Specific heat = 1.4

4.3.4 Flow Calculations Procedure

The flow output value conditions without any secondary flow injector at pressure values of 5, 10, 15, 20 and 25atm are calculated respectively. In comparison with the values obtained after using a secondary injector port which is used to make a fluidic membrane that prevents formation of any recirculation flow, that are obtained due to the flow separation accompanied by the atmospheric air getting sucked into the exhaust nozzle thereby creating a suction effect which affects the efficiency. Elimination of this phenomena is the sole purpose of using secondary injector in this project. This is theoretically proved in this paper by comparing the values used at the main nozzle conditions without any secondary injector, gets used here at the same nozzle along with a secondary injector. With only change in the secondary values that are obtained from the equation given above by assuming a factor value of 1.5.

5. RESULT

5.1 SIMULATION OF FLOW SEPARATION IN MAIN NOZZLE WITHOUT SECONDARY INJECTION

5.1.1 5 atm Main nozzle pressure inlet contours

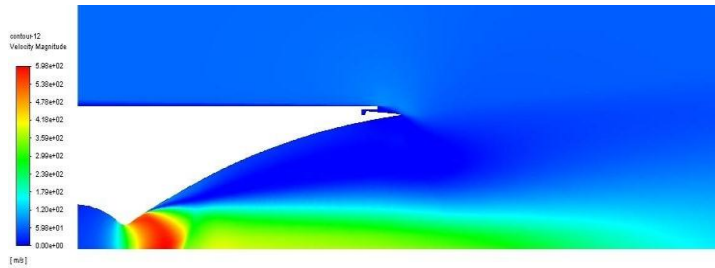


Fig-9: 5 atm main nozzle pressure inlet velocity magnitude

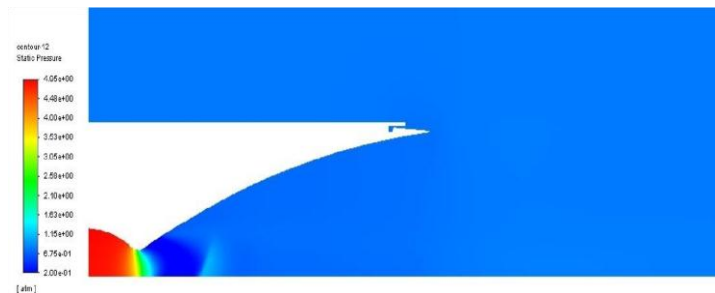


Fig-10: 5atm main nozzle pressure inlet static pressure

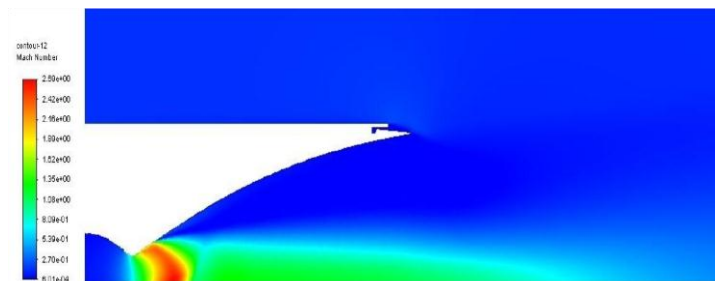


Fig-11: 5atm main nozzle pressure inlet mach number

5.1.2 10 atm Main nozzle pressure inlet contours

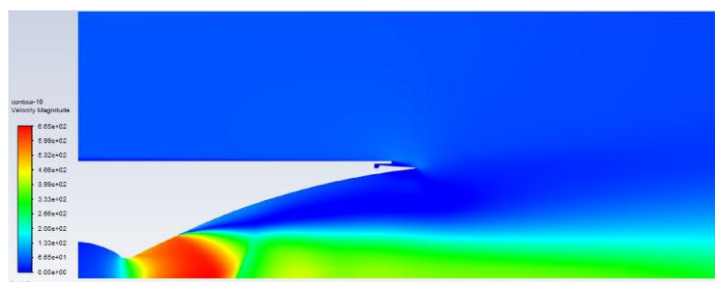


Fig-12: 10 atm main nozzle pressure inlet velocity magnitude



Fig-13: 10 atm main nozzle pressure inlet static pressure

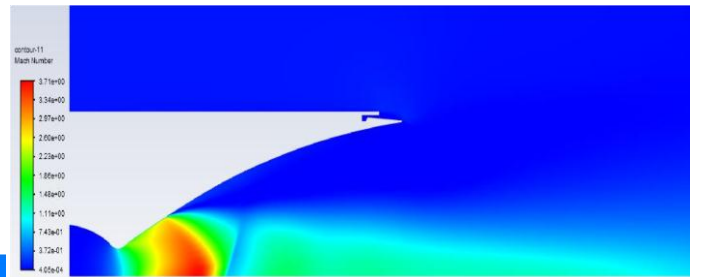


Fig-14: 10 atm main nozzle pressure inlet Mach number

5.1.3 15 atm Main nozzle pressure inlet contours

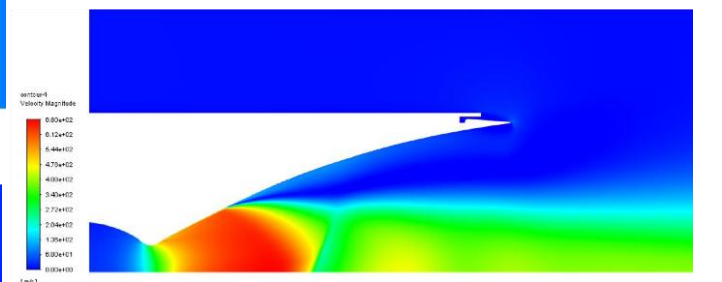


Fig-15: 15 atm main nozzle pressure inlet velocity magnitude



Fig-16: 15 atm main nozzle pressure inlet static pressure

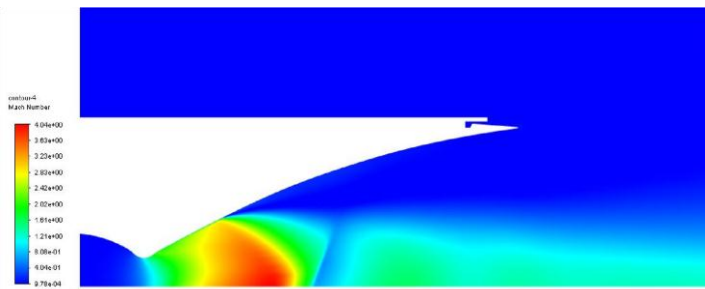


Fig-17: 15 atm main nozzle pressure inlet Mach number

5.1.5 25 atm Main Nozzle pressure inlet contours

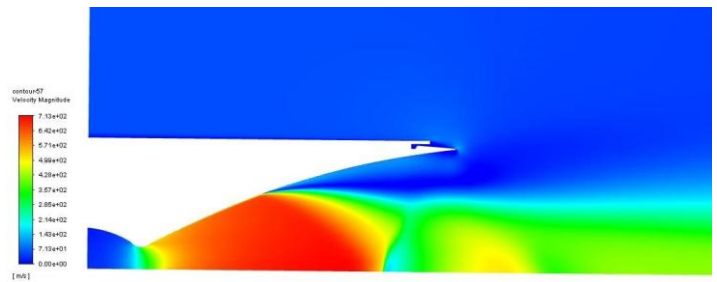


Fig-21: 25 atm main nozzle pressure inlet velocity magnitude

5.1.4 20 atm Main nozzle pressure inlet contours

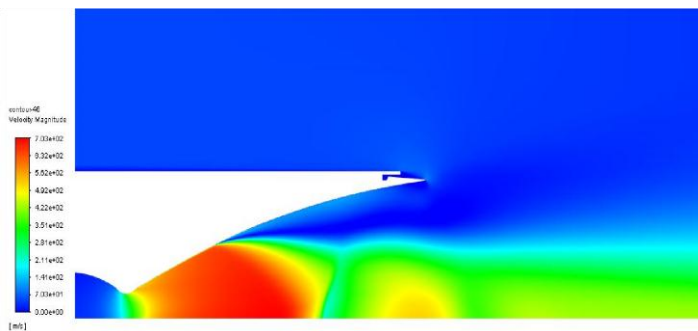


Fig-18: 20 atm main nozzle pressure inlet velocity magnitude

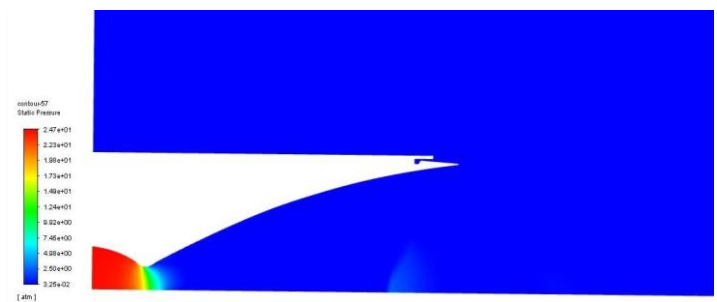


Fig-22: 25 atm main nozzle pressure inlet static pressure

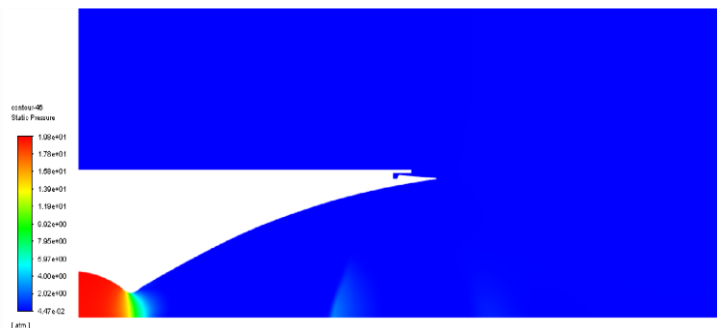


Fig-19: 20 atm main nozzle pressure inlet static pressure

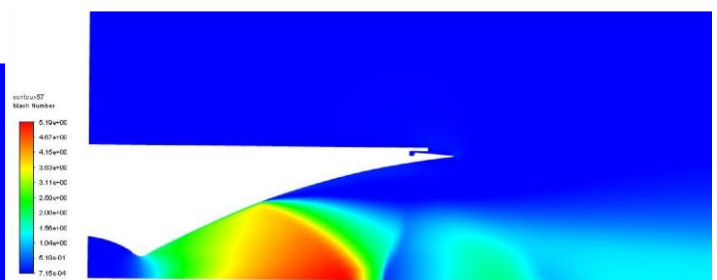


Fig-23: 25 atm main nozzle pressure inlet Mach number

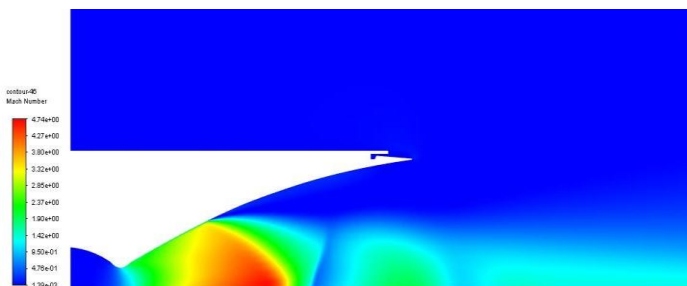


Fig-20: 20 atm main nozzle pressure inlet Mach number

5.2 SIMULATION OF FLOW SEPARATION IN MAIN NOZZLE WITH SECONDARY INJECTION AT MAIN NOZZLE EXHAUST LIP

5.2.1 5 atm main nozzle pressure inlet along with 2.5 atm secondary nozzle pressure inlet contours

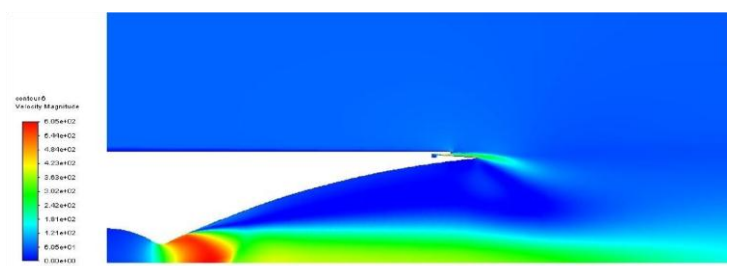


Fig-24: 5 atm main nozzle pressure inlet with 2.5 atm secondary nozzle pressure inlet - velocity magnitude

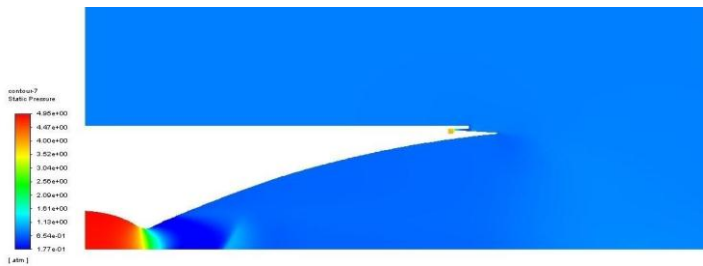


Fig-25: 5 atm main nozzle pressure inlet with 2.5 atm secondary nozzle pressure inlet - static pressure

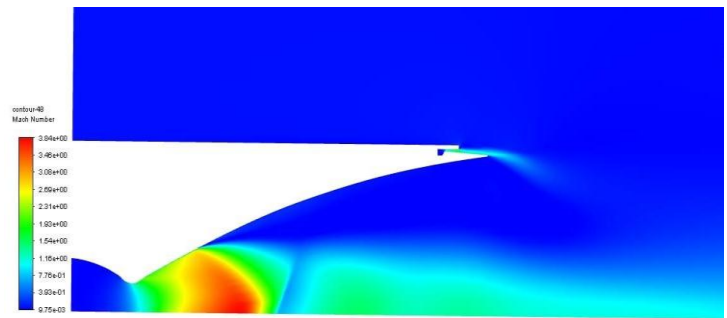


Fig-29: 10 atm main nozzle pressure inlet with 5 atm secondary nozzle pressure inlet - Mach number

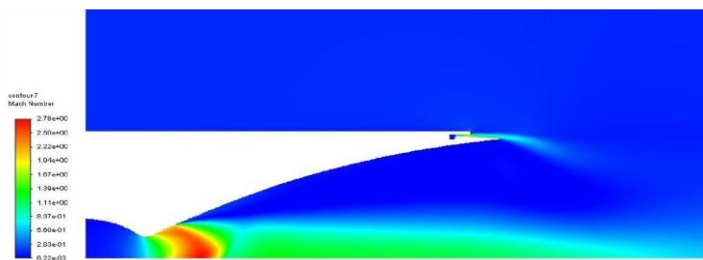


Fig-26: 5 atm main nozzle pressure inlet with 2.5 atm secondary nozzle pressure inlet - Mach number

5.2.3 15 atm main nozzle pressure inlet along with 7.5 atm secondary nozzle pressure inlet contours

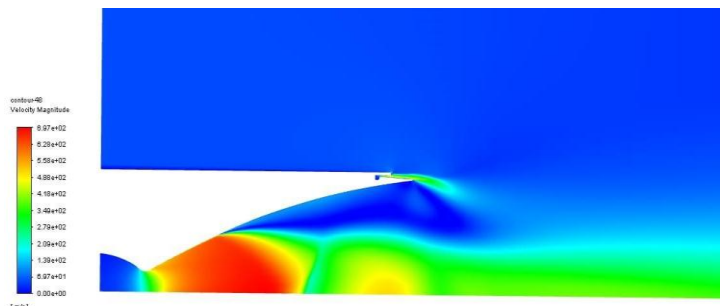


Fig -30: 15 atm main nozzle pressure inlet with 7.5 atm secondary nozzle pressure inlet- velocity magnitude

5.2.2 10 atm main nozzle pressure inlet along with 5 atm secondary nozzle pressure inlet contours

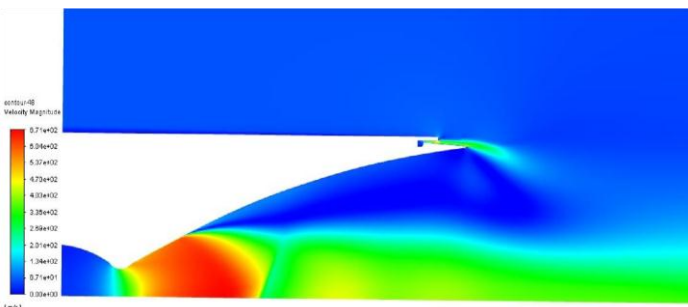


Fig- 27: 10 atm main nozzle pressure inlet with 5 atm secondary nozzle pressure inlet - velocity magnitude

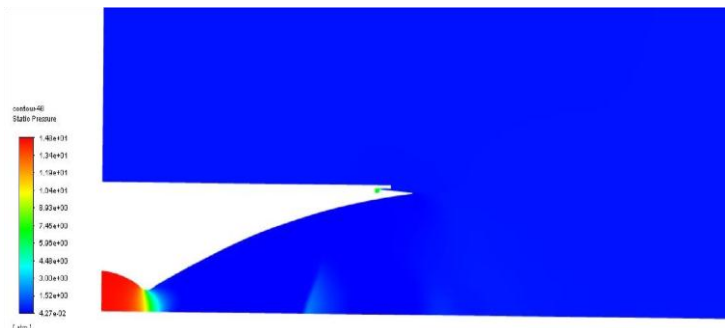


Fig-31: 15 atm main nozzle pressure inlet with 7.5 atm secondary nozzle pressure inlet - static pressure

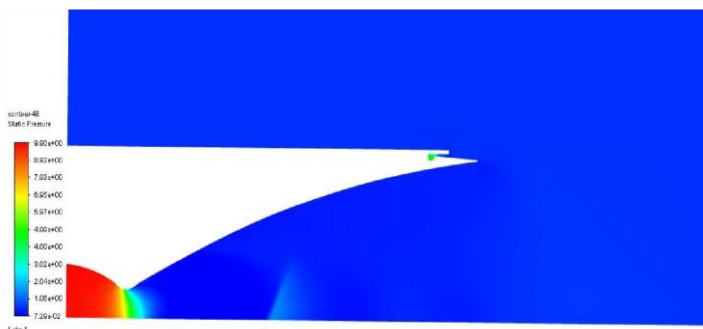


Fig-28: 10 atm main nozzle pressure inlet with 5 atm secondary nozzle pressure inlet - static pressure

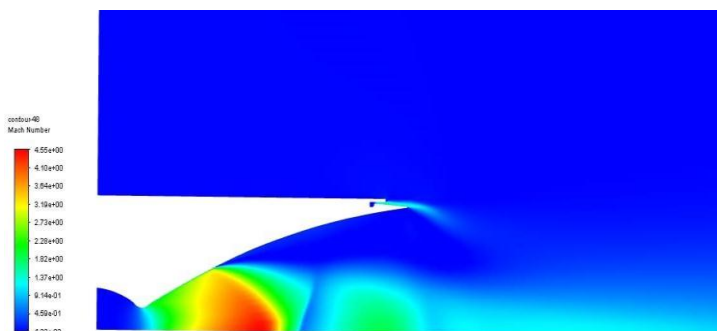


Fig-32: 15 atm main nozzle pressure inlet with 7.5 atm secondary nozzle pressure inlet - Mach number

5.2.4 20 atm main nozzle pressure inlet along with 10 atm secondary nozzle pressure inlet contours

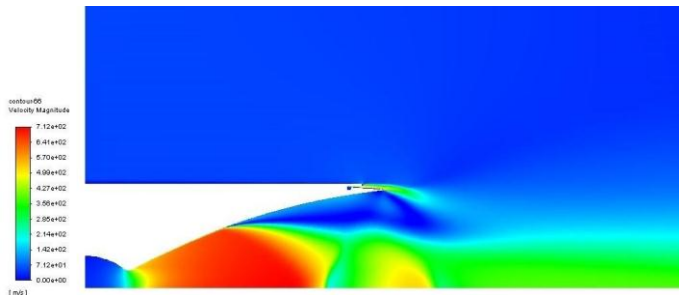


Fig-33: 20 atm main nozzle pressure inlet with 10 atm secondary nozzle pressure inlet - velocity magnitude

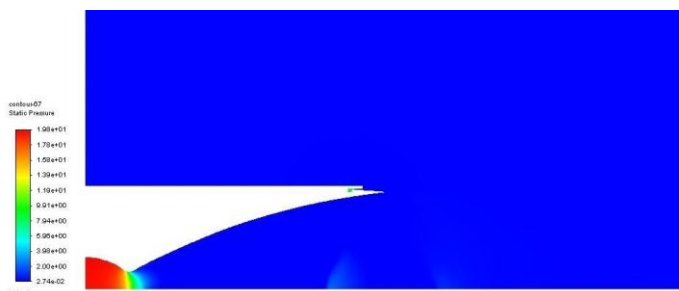


Fig-34: 20 atm main nozzle pressure inlet with 10 atm secondary nozzle pressure inlet - static pressure

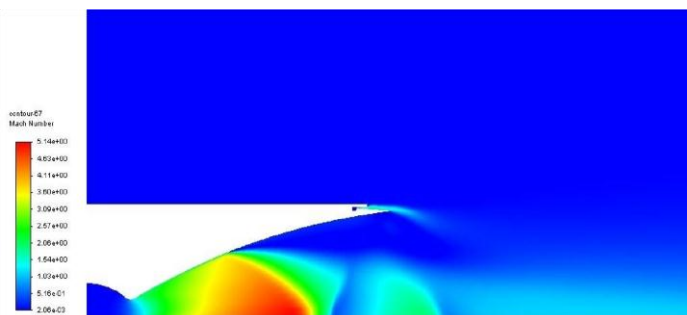


Fig-35: 20 atm main nozzle pressure inlet with 10 atm secondary nozzle pressure inlet - Mach number

5.2.5 25 atm main nozzle pressure inlet along with 12.5 atm secondary nozzle pressure inlet contours

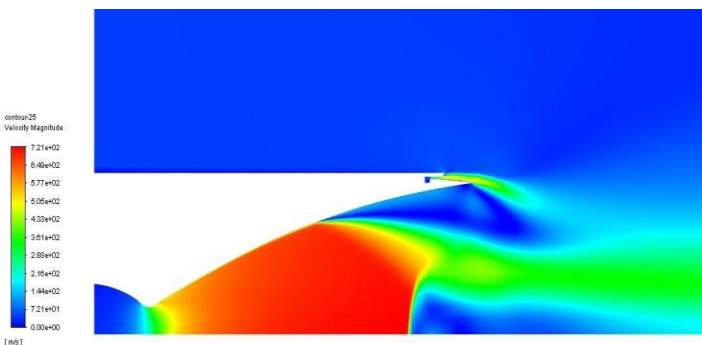


Fig-36: 25 atm main nozzle pressure inlet with 12.5 atm secondary nozzle pressure inlet - velocity magnitude

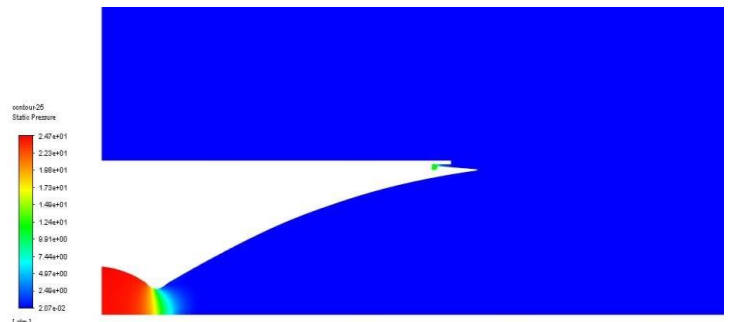


Fig-37: 25 atm main nozzle pressure inlet with 12.5 atm secondary nozzle pressure inlet - static pressure

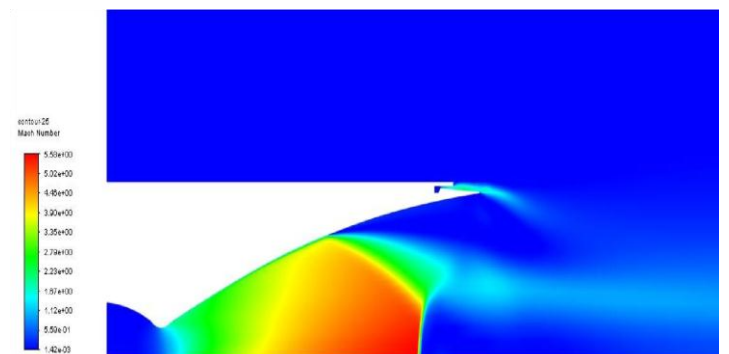


Fig-38: 25 atm main nozzle pressure inlet with 12.5 atm secondary nozzle pressure inlet - Mach number

6. COMPARISON

6.1 Static Pressure Comparison

Graphical representation with static pressure on y-axis w.r.t the main nozzle wall on x-axis taken from our simulation analysis. Both the conditions involving with and without secondary flow injection is compared below:

6.1.1- 5 atm main nozzle pressure inlet vs 5 atm main nozzle pressure inlet with 2.5 atm secondary nozzle pressure inlet

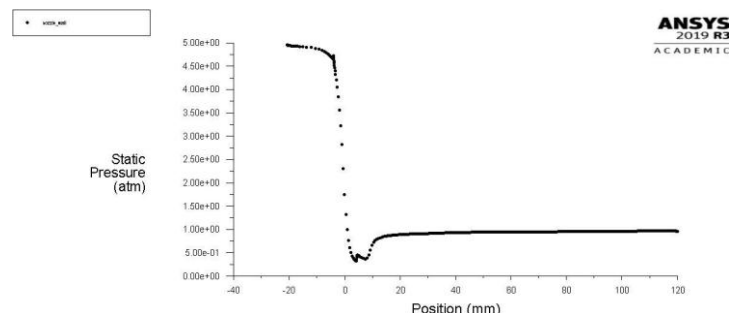


Chart -1: 5 atm main nozzle pressure inlet static pressure graph w.r.t main nozzle wall

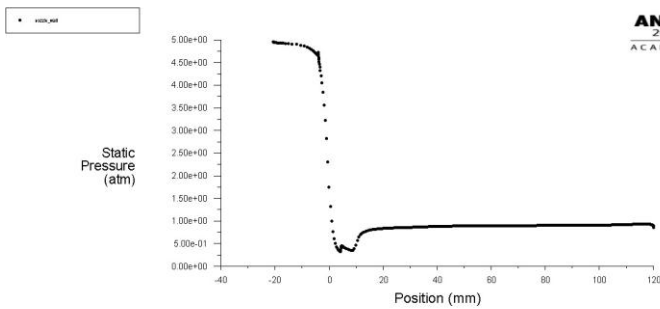


Chart-2: 5 atm main nozzle pressure inlet with 2.5 atm secondary nozzle pressure inlet - static pressure graph w.r.t main nozzle wall.

Results from above figures are; Max static pressure – 4.95 atm. The flow separation starts at 10 mm aft the throat section in both cases. No changes in flow separation point can be seen here.

6.1.2 -10 atm main nozzle pressure inlet vs 10 atm main nozzle pressure inlet with 5 atm secondary nozzle pressure inlet

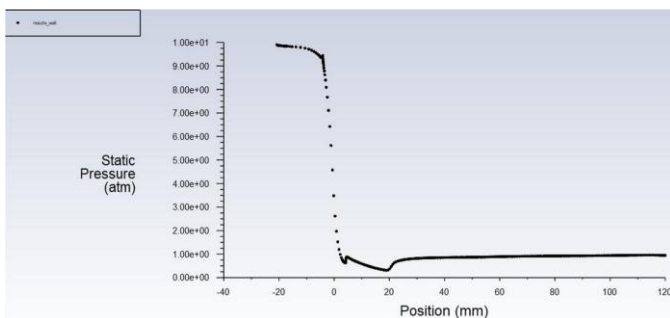


Chart- 3: 10 atm main nozzle pressure inlet static pressure graph w.r.t main nozzle wall

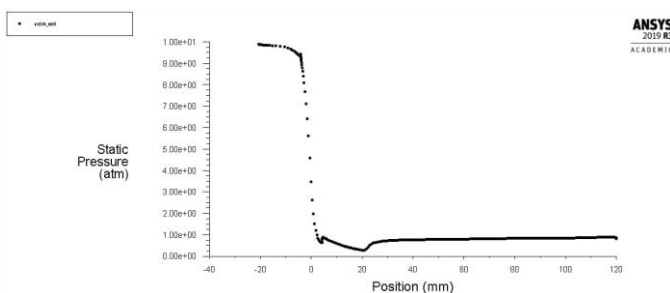


Chart-4: 10 atm main nozzle pressure inlet with 5 atm secondary nozzle pressure inlet - static pressure graph w.r.t main nozzle wall

Results from above figures are; Max static pressure – 9.90 atm. The flow separation starts at 20 mm aft the throat section in both cases. No sensitive changes can be seen here.

6.1.3 -15 atm main nozzle pressure inlet vs 15 atm main nozzle pressure inlet along with 7.5 atm secondary nozzle pressure inlet

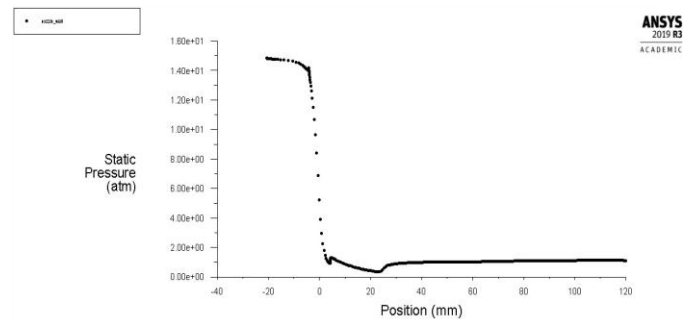


Chart -5: 15 atm main nozzle pressure inlet static pressure graph w.r.t main nozzle wall

The max static pressure is 14.8 atm and flow separation starts at 20 mm aft the throat section, without any secondary pressure inlet.

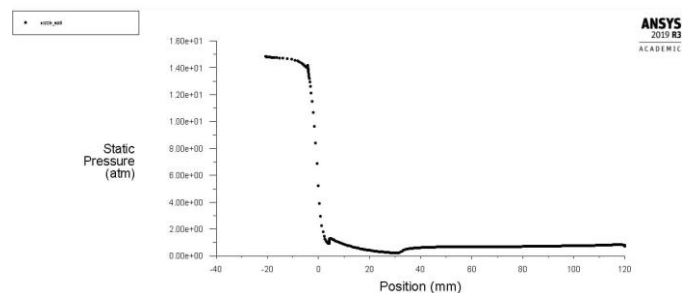


Chart 6: 15 atm main nozzle pressure inlet with 7.5 atm secondary nozzle pressure inlet - static pressure graph w.r.t main nozzle wall.

When a secondary flow of 7.5 atm is introduced, then flow separation point shifts to 35 mm aft the throat section.

Approximately the flow separation shifts 15 mm due to secondary injection.

6.1.4- 20 atm main nozzle pressure inlet vs 20 atm main nozzle pressure inlet along with 10 atm secondary pressure inlet

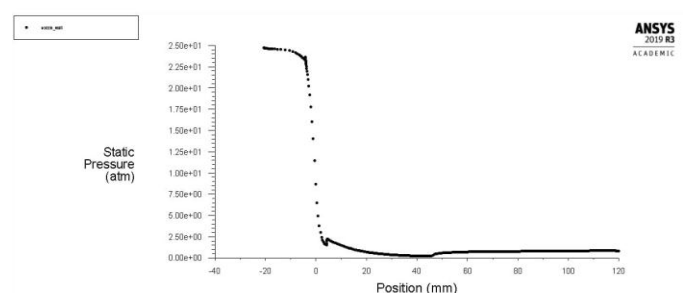


Chart -7: 20 atm main nozzle pressure inlet static pressure graph w.r.t main nozzle wall

Above figure shows a max static pressure of 19.8 atm, and the flow get separated at 35 mm aft throat section.

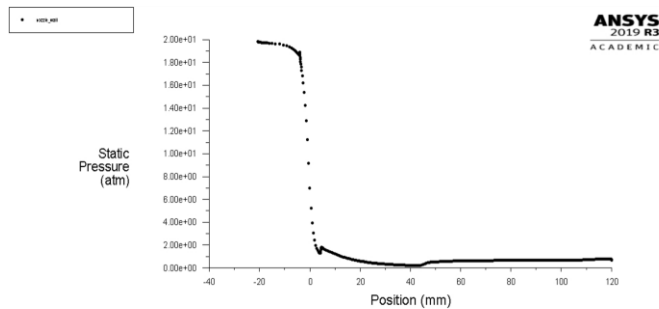


Chart-8: 20atm main nozzle pressure inlet with 10atm secondary nozzle pressure inlet - static pressure graph w.r.t main nozzle wall.

When a secondary flow of 10atm is introduced, then flow separation shifts to 45mm aft the throat section.

Approximately the flow separation shifts 10 mm due to secondary injection.

6.1.5- 25 atm main nozzle pressure inlet vs 25 atm main nozzle pressure inlet along with 12.5 atm secondary pressure inlet

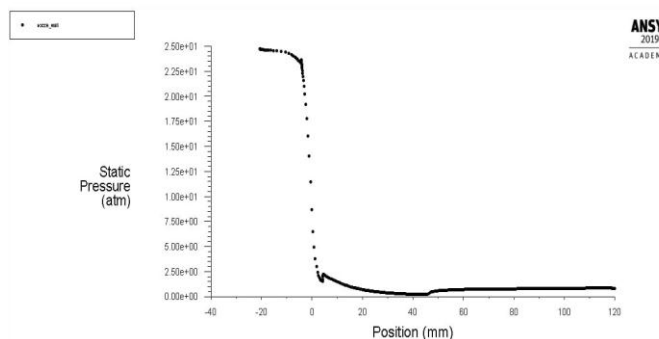


Chart -9: 25atm main nozzle pressure inlet static pressure graph w.r.t main nozzle wall

The max static pressure – 24.5atm and flow separation starts at 45 mm aft the throat section, without any secondary pressure inlet.

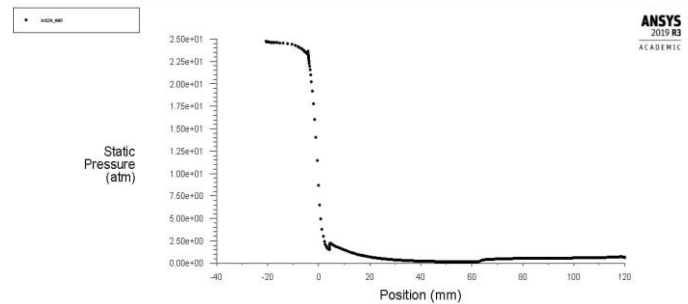


Chart-10: 25 atm main nozzle pressure inlet with 12.5 atm secondary nozzle pressure inlet - static pressure graph w.r.t main nozzle wall.

When a secondary flow of 12.5 atm is introduced, the flow separation point gets shifted to 62.5 mm aft throat section.

Approximately the flow separation point shifts 17.5 mm due to secondary injection.

6.1 Mach Number Comparison

The Mach number data of the flow taken from the simulation for both the conditions involving with and without secondary injection is taken and compared below:

Main nozzle pressure inlet	Secondary nozzle pressure inlet	Mach number
5atm		2.69
5atm	2.5atm	2.78
10atm		3.71
10atm	5atm	3.84
15atm		4.04
15atm	7.5atm	4.50
20atm		4.74
20 atm	10 atm	5.14
25 atm		5.19
25 atm	12.5 atm	5.58

Table-1: Mach number comparisons

The data compared shows increase in the Mach number when secondary injection is provided.

7. CONCLUSIONS

The simulation consisted of using air as the working fluid for both main nozzle and secondary injection nozzles. The inlet pressure condition provided for the main nozzle were 5 atm, 10 atm, 15 atm, 20 atm and 25 atm. The secondary nozzle inlet pressure condition provided were 2.5 atm, 5 atm, 7.5 atm, 10 atm and 12.5 atm respectively. The results yielded by the simulation shows that by introducing a secondary injection, the flow separation point shifts downstream the flow. The downstream shifting of this separation indicates improvement in nozzle flow expansion which further

indicates improved performance and reduced side loads compared to non – secondary injection condition.

The complete flow attachment in the divergent section nozzle wall can be ensured by proper designing of both the convergent and the divergent section. The design of the secondary injection exhaust contour and the main nozzle exhaust lip has an important role to play in ensuring complete flow attachment in main nozzle. More experimental and simulation researches should be carried out in testing different potential fluids that can be used in secondary injection. The coaxial secondary injection system is the best way to control the flow separation in nozzle owing to its simple working and lack of any complex machineries or systems. The rocket engine having such system can have a wide throttling range in different altitudes without incurring flow separation and associated side loads. This system can also be incorporated in rockets for thrust vectoring purposes.

REFERENCES

- [1] Luca Boccaletto, François Cahuzac (2008), solving the flow separation issue: a new nozzle concept, 44th AIAA/ASME/SAE/ASEE Joint Propulsion conference & exhibit.
- [2] Beena D. Baloni, Sonu P. Kumar, S.A. Channiwala (2017), Computational analysis of bell nozzles, 4th International Conference of Fluid Flow Heat and Mass Transfer (FFHMT'17).
- [3] Rokas Simions and Dr. Bidur Khanal, Axisymmetric simulation of a rocket mortar exhaust in Ansys Fluent <http://simions.coventry.domains/cfd/axisymmetric-simulation-of-a-rocket-mortar-exhaust-in-ansys-fluent-dissertation-project-2/>
- [4] Ralf H. Stark (2005), Flow separation in rocket nozzles: A simple criterion, 41st AIAA/ASME/SAE/ASEE Joint Propulsion Conference & Exhibit.
- [5] M. Frey and G. Hagemann (2012), Status of flow separation prediction in rocket nozzles, Aerospace Research Central.
- [6] Abdellah Hadjadj, Marcello Onofori (2009), Nozzle flow separation, Springer-Verlag.
- [7] Ralf H. Stark (2005), Flow separation in rocket nozzles: A simple criteria, 41st AIAA/ASME/SAE/ASEE Joint Propulsion Conference & Exhibit.